A regenerative braking system for internal combustion engine vehicles based on supercapacitors. Part 2: Simulation results

Emiliano Pipitone[a], Gianpaolo Vitale[b,*]

[a] Department of Engineering, University of Palermo, Italy

[b] ICAR, Institute for high performance computing and networking, National Research Council of Italy

[*] Corresponding author: gianpaolo.vitale@icar.cnr.it

Abstract: In this two-parts work an electric Kinetic Energy Recovery System (e-KERS) for internal combustion engine vehicle (ICEV) is presented and its performance evaluated through numerical simulations. The KERS proposed is based on the use of supercapacitors as energy storage, interfaced to a brushless machine through a properly designed power converter. In part 1 the system is described and analyzed, and the mathematical model used for the simulations is presented. For each component of the KERS, the real efficiency and the power or energy limitations are adequately considered. In part 2 the energetic and economic advantages attainable by the proposed KERS are evaluated using MATLAB Simulink, considering a widely diffused gasoline passenger car and two reference driving cycles (ECE-15 and Artemis Urban). Energy savings of the order of 16% were found, with a slight increase in vehicle weight (+2%) and with an overall commercial cost that would be compensated in 7 years thanks to the fuel economy improvement, to which corresponds an equal reduction of CO_2 emissions. The low complexity of the system, never proposed for ICEV, the moderate weight of its components and their availability on the market, make the solution presented ready for the introduction in current vehicle production.

Keywords: Kinetic Energy Recovery System; Supercapacitor; Ultracapacitor; Vehicle Fuel economy; Regenerative Braking; Urban Driving Cycle; Hybrid Vehicle;

8 Introduction

In the first part of this two-papers work [43] the authors presented and described an electric Kinetic Energy Recovery System (e-KERS) for internal combustion engine vehicles (ICEV). The e-KERS is schematically represented in Figure 6 together with the vehicle drivetrain: the supercapacitors bank (SC) is the energy storage of the system and is

electrically interfaced, by means of an expressly designed power converter (PC), to a motor-generator unit (MGU) which is mechanically connected to the drive shaft via a fixed gear ratio and converts the vehicle kinetic energy into electric energy and vice versa; the system was conceived to recover the vehicle kinetic energy during braking phases by charging the supercapacitor, whose stored energy is employed by the MGU for successive vehicle acceleration thus lowering the power demand to the thermal engine, with the consequent obvious advantages in terms of reduced fuel consumption and air pollution. In the same paper Part 1 the authors also presented a mathematical model developed for the evaluation of the performance provided by the proposed e-KERS by means of numerical simulations; for each component of the KERS, the model adequately takes into consideration the real efficiency as well as the power or energy limitations.

The purpose of this second part paper is to evaluate the energetic performances and economic advantages connected to the implementation of the proposed KERS in a passenger car. In effect the use of a SC as single energy storage element has been proposed only when large spaces and weight were allowed, as for example in the case of electric city rail [44] or hybrid city bus [45], where energy saving of about 40% were obtained. In the present study, instead, the authors aim to evaluate the plausible reduction of fuel consumption, and related CO_2 emissions, that could be achieved by the implementation of the electric KERS proposed in traditional passenger cars endowed of Internal Combustion Engine (ICE), with the aim to improve their sustainability and environmental compatibility. The system proposed in this paper may contribute to their hybridization process of ICEV, already started with the development of the so called starter-generators system [46], whose growth in power, control complexity and launching ability could further promote the use of supercapacitors as energy storage elements for KERS application.

9 KERS sizing

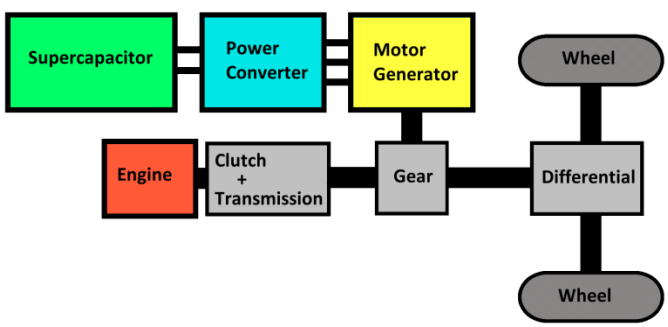

Figure 6 Drivetrain layout of the vehicle with KERS

The effectiveness of the KERS proposed in reducing the vehicle energy demand was evaluated considering one of the most diffused passenger car in Europe [47], whose main characteristics are reported in Table 1.

Table 1 Characteristic parameters of the vehicle considered in this study

Brand and model		Volkswagen Golf 1.4 TSI
Segment		C – Medium cars
Reference mass	[kg]	1315
Engine displacement	[L]	1.39
Maximum output power	[kW]	90
Homologation		Euro 5
Drag coefficient	c_x	0.28
Frontal surface area	[m^2]	2.63
Fuel		Gasoline
Fuel LHV	[MJ kg^{-1}]	43.4
Fuel density	[kg m^{-3}]	730
Tyres		205/55R16
Wheel radius	[m]	0.519
Differential gear ratio	τ_d	3.65

Table 2 Measured energy consumption and CO_2 emissions on both driving cycles considered [48]

		ECE-15	Artemis Urban
Cycle length	[km]	0.995	4.87
Fuel consumption	[L (100 km)$^{-1}$]	8.30	10.3
CO_2 emissions	[g km^{-1}]	193	239

As can be noted, the vehicle is characterized by a 1.4 L gasoline fuelled engine and by a reference mass (i.e. including fuel, with an addition of 100 kg to account for driver and luggage, as prescribed by EU directive 95/48) of 1315 kg, which are average values in the typical range for passenger cars employed in urban context.

Table 2 reports the fuel consumption and CO_2 emissions experimentally measured on the vehicle considered [48] with regards to two different standard driving cycles: the ECE-15 and the Artemis Urban. Standard driving cycles are the type approval test carried out to evaluate the air pollution and fuel consumption of vehicles equipped with internal combustion engines. The procedure consists in reproducing on a roller test bench a typical vehicle speed profile as function of time, with the aim to simulate the vehicle usage both in urban and extra-urban area and to measure the resulting air pollution and fuel consumption. There are several commonly used driving test cycles all over the world [49][50]. For more than 20 years the European Union adopted the so called New European Driving Cycle (NEDC), composed of four repetitions of the ECE-15, used to simulate vehicle use in urban area (also known as UDC, i.e. Urban Driving Cycle), and a single repetition of the Extra Urban Driving Cycle (EUDC), which instead was dedicated to the extra urban use of the vehicle. The mentioned European driving cycle was however considered unable to reproduce the

real vehicle use, above all in the urban conditions [49][50], because of the few (and too mild) transient phases which compose the cycles. This led to the study and development of alternative driving cycles, more representative of the real vehicle use, such as the ARTEMIS cycles [51], which is also divided in Urban, Road and Motorway parts, and the more recent Worldwide harmonized Light vehicles Test Cycles (WLTC), which, after the transition phase 2017-2019, will definitively replace the NEDC cycle in all the UNECE member states for vehicle test approval [52]. Since a kinetic energy recovery system reveals effective only in urban application, where the vehicle accelerations may be obtained by exploiting the energy recovered during the braking phases, the authors focused on the urban driving cycles for the design of the KERS and for the evaluation of its performances; based on the availability of measured fuel consumption data [48], the European ECE-15 driving cycle and the Artemis Urban driving cycle, reproduced in Figure 7, were taken into consideration.

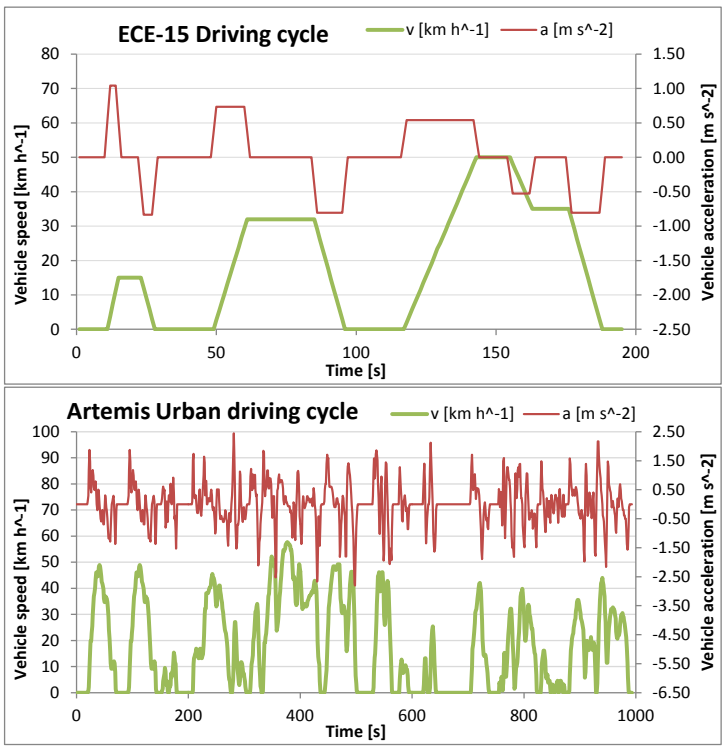

Figure 7 Speed and acceleration profile of the ECE-15 cycle (upper) and Artemis urban cycle (lower)

Obviously, each KERS component must be able to manage the power connected to the vehicle transient phases (acceleration or braking phases), and this means that the speed of variation of the vehicle kinetic energy constitutes a power sizing factor for each KERS element. Furthermore, the storage capacity of the supercapacitor should be able to adequately face up the vehicle kinetic energy variation. The kinetic energy recovery system must hence fulfil two separate conditions: the first regards the maximum energy that can be stored or supplied, and the second regards the maximum power to be managed. These two constraints bind the design of the power conversion chain, i.e. the size of each element of the KERS.

As regards the first condition required for KERS sizing, i.e. the maximum storable energy, the authors considered that the supercapacitor cannot supply to the MGU energy that has not been previously stored during previous braking phases; according to this observation, the authors determined the maximum storable energy on the basis of the braking phases of the driving cycle, ignoring, for the purpose, the acceleration phases.

Neglecting, for the moment, the efficiency of the KERS components, the total amount of energy E_{br} that could be recovered during a braking phase can be estimated as the integral of the braking power P_{br} during the whole braking period:

$$E_{br} = \int_{braking} P_{br}(t)\,dt = \int_{braking} [-P_{road}(t) - m_v \cdot a(t) \cdot v(t)]\,dt \tag{57}$$

It is worth to point out that two or more successive braking phases, without intermediate acceleration phases, allow to store the sum of the energy recovered by each single phase. The recoverable energy was then evaluated for the vehicle considered on both ECE-15 and Artemis Urban driving cycles, as reported in Figure 8.

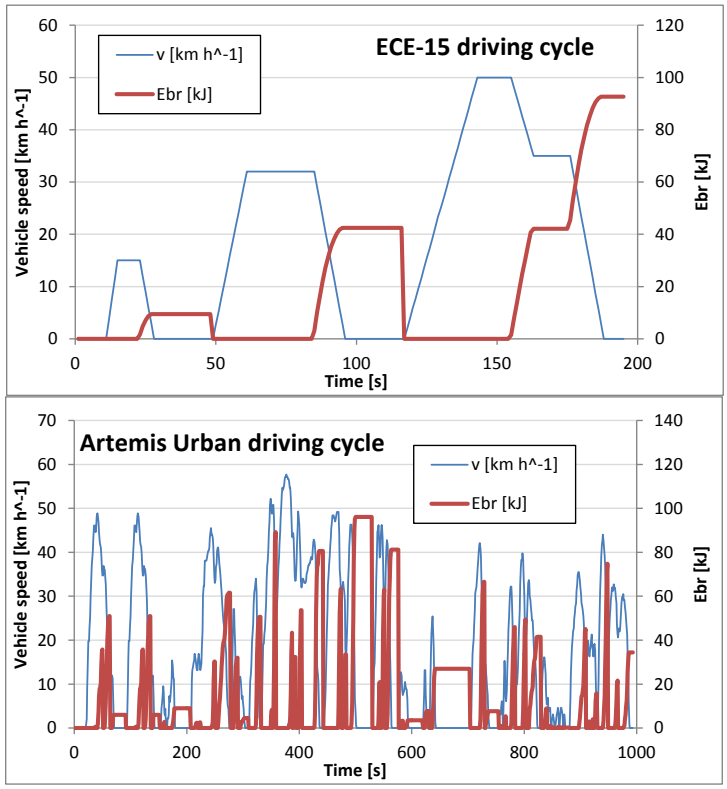

Figure 8 Energy recoverable E_{br} in the braking phases of the ECE-15 cycle (upper) and of the Artemis urban cycle (lower)

The resulting values of the maximum storable energy are reported in Table 3: as can be observed, for the vehicle considered, the required capacity of the energy storage should be around 100 kJ, a part from the urban driving cycle adopted: this is quite an interesting result, since establishes a sort of equivalence between ECE-15 and Artemis Urban driving cycles. Two factors must be however considered:

1. as mentioned, the evaluation carried out does not take into account the energy conversion efficiencies of the real components of the KERS, which will instead properly considered further on in the simulations, once the KERS components have been selected

2. as shown in the description of the Simulink model, being the minimum working voltage of the SC about 20% of the nominal value, the supercapacitor cannot entirely exploit its nominal capacity

In consideration of both factors, the author increased by 20% the minimum required energy storage capacity, which was hence assumed to be at least 120 kJ.

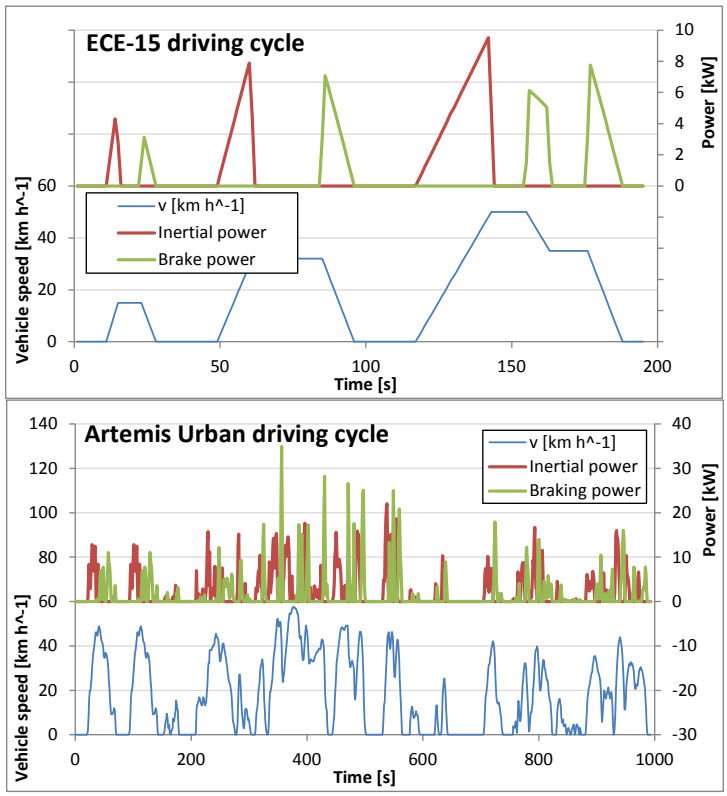

Figure 9 Inertial power P_I and braking power P_{br} in the ECE-15 cycle (upper) and in the Artemis Urban cycle (lower)

As regards the second constraint, the rated power of each KERS components should be related to the inertial power P_I required during the accelerations and to the recoverable power P_{br} during the braking phases of the vehicle, both reported, for the vehicle considered, in Figure 9 for the ECE-15 and for the Artemis Urban cycle: as can be noted, differently from the maximum recoverable energy, the two urban cycles show noticeable differences in terms of maximum power values: as resumed in Table 3, according to the Artemis Urban cycle, the KERS should manage the power of 34.9 kW, while 12.7 kW would be sufficient if the ECE-15 cycle is considered. In consideration of the substantial difference between the power requirements emerged by the two urban cycles, the authors decided to take into consideration four KERS of different power sizes, with the aim to determine, through simulations, the optimal choice.

The same Table 3 also shows the mean values of the power that the KERS should manage, evaluated considering the inertial power P_I and the recoverable power P_{br} during the whole driving cycle: as can be noted, this time the two urban driving cycles produce similar results.

Table 3 Maximum KERS power and maximum recoverable energy evaluated on both ECE-15 and Artemis Urban cycles (for the vehicle considered in Table 1)

Maximum recoverable energy [kJ]		Maximum transient power [kW]		Mean transient power [kW]	
ECE-15	Artemis Urban	ECE-15	Artemis Urban	ECE-15	Artemis Urban
92.7	96.2	12.7	34.9	4.26	5.24

The design of the KERS proposed in this work was carried out considering solutions with the minimum impact on the vehicle weight, focusing on products already available on the market, which also allowed to evaluate the related costs. Given the minimum energy requirements determined in the previous section (i.e. 120 kJ), the authors selected the supercapacitor Green Tech GTSM-48V165FUS, whose main characteristics [53] and commercial cost are reported in Table 4. As shown, the energy storable by this supercapacitor amply satisfies the requirement. As regards the power output, the supercapacitor datasheet reports a maximum allowed current of 2275A, which, at the rated voltage of 48 V, means a maximum allowed power of 109 kW, which is quite above the highest power requirement (35 kW in Table 3).

Table 4 Supercapacitor selected from the available product on the market [53]

Brand		Green Tech
Model		GTSM-48V165FUS
Capacitance C	[F]	165
Rated voltage $V_{SC,max}$	[V]	48
Storable energy $E_{SC,max}$	[kJ]	190.1
Maximum Current	[A]	2275
ESR	[mΩ]	5
Weight	[kg]	14.5
Commercial cost	[€]	602

It must be pointed out, however, that the real maximum available power of the supercapacitor is

$$P_{SC,max}(t) = V_{SC}(t) \cdot i_{PC,max} \tag{58}$$

and depends on the instantaneous working voltage $V_{SC}(t)$ of the supercapacitor, which continuously vary during KERS operation together with the amount of energy stored, and on the maximum current allowed in the power converter $i_{PC,max}$, which, as shown further on, will be properly determined to meet the power requirement.

As regards the motor generator units, the author focused on compact, open frame, fan cooled three phases brushless motors, which are available on the market with adequate power size [54][55]: according to the range of output power identified in the previous section (from 12.7 kW to 34.9 kW, as reported in Table 3) the authors selected the four products listed in Table 5.

Table 5 Motor generator units selected from the available products on the market [54][55]

Brand	MOTENERGY			
Model	ME1305	ME1117	ME1114	ME1115
Max DC voltage $V_{MGU,max}$ [V]	72	72	72	96
Continuous motor power [kW]	4.4	4.4	10.0	12.0
Continuous input DC current [A]	100	120	180	180
Peak motor power [kW]	11.0	14.0	24.0	30.0
Peak DC current $i_{MGU,max}$ [A]	230	300	600	600
Peak stall torque $T_{MGU,stall}$ [Nm]	38.0	38.0	65.1	81.3
Max speed $n_{MGU,max}$ [rpm]	5000	5000	5000	5000
Weight [kg]	10.0	10.0	15.9	15.9
Rotor inertia [kg cm2]	52.0	52.0	45.0	45.0
Max Efficiency	0.90	0.90	0.92	0.92
Commercial cost [€]	527	544	606	606

As can be observed, the selected motors can deliver, for a period not exceeding 30 seconds, peak power from 11 to 30 kW (involving the related peak current levels), which comply with the requirements, even if the allowed continuous power level are 2.4 to 3 times lower: this is a fundamental feature, since allow the selected machines to fulfil the vehicle transient phases (usually shorter than 30 seconds), while maintaining the reasonable weights and costs of low power machines. The maximum torque $T_{MGU,max}$ that can be delivered as motor (or received as generator) without causing overheating or demagnetization of the permanent magnets, ranges from 38 to 81 Nm. As already pointed out in paper Part 1, this kind of brushless motor needs a proper controller (which, in the system proposed, is embedded into the power converter of Figure 6) to transforms DC into AC power and supply the motor with proper sinusoidal waveforms. Moreover, as already stated, the brushless motor is assumed to be current-controlled, i.e. the torque delivered (or received) is controlled by controlling the phase-currents, as described in [56]: this task is obviously accomplished by the power converter, which was properly designed for the purpose [57]. The maximum speed of revolution of all the motor selected does not allow a direct connection with the drive shaft, making hence necessary the adoption of a gear drive, whose efficiency η_G (supposed 0.97 in this paper) will certainly condition the overall KERS efficiency and will be properly taken into account in the numerical simulations. With an optimized suitable design, the MGU could be coaxial with drive shaft, eliminating hence the necessity of a gear and increasing the overall KERS

efficiency. As already mentioned in paper Part 1, the brushless gear ratio τ_G was fixed considering to reach the maximum motor rotation speed at the vehicle speed of 60 km h^{-1}.

Once selected the supercapacitor and the motor-generator units, the power converter of each KERS can be adequately sized to manage the power transfer during both acceleration and braking transients. Considering the structure of the KERS proposed (see Figure 6), the power flux involving each element is schematically reported in Figure 10 both for an acceleration and for a braking phase; this diagram helps to identify the magnitude of the power managed by each component of the KERS, such as the power converter.

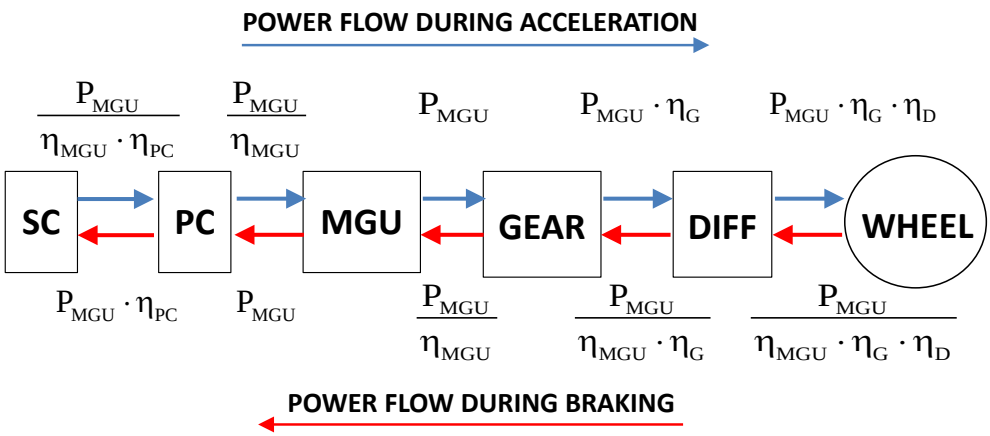

Figure 10 Schematic representation of the KERS power fluxes in both acceleration and braking phase

As shown in Figure 10, during vehicle acceleration, the PC should be able to deliver the power (P_{MGU}/η_{MGU}) to the MGU, while during a braking phase the PC should transmit the power ($P_{MGU}\cdot\eta_{PC}$) to the supercapacitor, being η_{PC} the efficiency of the power converter: it is hence clear that the power converter will manage the maximum power levels during the acceleration process, and its maximum output power $P_{PC,max}$ is determined by the maximum input power to the MGU, which, in turns, depends on the maximum allowed current and voltage on the DC side of the MGU controller:

$$P_{PC,\max} = V_{MGU,\max}\cdot i_{MGU,\max} \tag{59}$$

The data reported in Table 5 allow to determine the maximum output power $P_{PC,max}$ of the power converter, for each brushless machine considered. As already shown in in Figure 3 of paper Part 1, the efficiency curve of such a power converter [57] reveals that for power factor exceeding 10% of the maximum, the efficiency remains at its best value, i.e. 0.93.

The maximum allowed DC current in the power converter $i_{PC,max}$ was determined on the basis of two considerations:

1) as already mentioned, the vehicle acceleration phases involve the highest power levels in the power converter; as clear from the power fluxes in Figure 10, during vehicle acceleration the PC deliver the power (P_{MGU}/η_{MGU}) to the MGU, receiving the power ($P_{MGU}/\eta_{MGU}/\eta_{PC}$) from the supercapacitor.

2) the PC works on two different voltage levels: on one side, it exchanges power with the supercapacitor, whose working voltage $V_{SC}(t)$ depends on the amount of energy stored and may reach the maximum value $V_{SC,max}$ (48 V for the model considered, as reported in Table 4); on the other side, the PC exchanges power with the MGU, which, in this work, is supposed to work always at its maximum voltage level $V_{MGU,max}$ (from 72 to 96 V, as reported in Table 5) with the aim to maintain as low as possible the current involved and the related losses.

It results that, for the power converter of the system considered, the working current on the supercapacitor side is always higher than the current on the DC side of the MGU:

$$i_{SC}(t) = \frac{P_{MGU}(t)}{\eta_{MGU}(t) \cdot \eta_{PC}(t) \cdot V_{SC}(t)} > \frac{P_{MGU}(t)}{\eta_{MGU}(t) \cdot V_{MGU,\max}} = i_{MGU}(t) \tag{60}$$

Hence the power converter of each KERS was sized to manage the maximum allowed current:

$$i_{PC,\max} = \frac{P_{PC,in,\max}}{V_{SC,\max}} = \frac{P_{PC,\max}}{\eta_{PC}^{*} \cdot V_{SC,\max}} = \frac{P_{MGU,\text{in},\max}}{\eta_{PC}^{*} \cdot V_{SC,\max}} \tag{61}$$

being $P_{PC,in,max}$ the maximum input power to the power converter, evaluated through its efficiency at the maximum output power η_{PC}* (0.93, as reported in Figure 3 of paper Part 1). Summing up, the specifications of the power converters of each KERS considered in this work are reported in Table 6.

Table 6 Power converter specifications for each of the four KERS considered

	KERS1	KERS2	KERS3	KERS4
Peak motor power [kW]	11.0	14.0	24.0	30.0
Max output power $P_{PC,max}$ [kW]	16.56	21.60	43.20	57.60
Max current $i_{PC,max}$ [A]	371	484	968	1290
Max efficiency	0.93	0.93	0.93	0.93
Max input power $P_{PC,in,max}$ [kW]	17.8	23.2	46.5	61.9
Weight [kg]	2.30	3.00	6.00	8.00
Commercial cost [€]	360	469	938	1251

It is worth to point out that the maximum allowed current determined for each power converter is lower than the maximum current allowed by the supercapacitor (2275A in Table 4) and put a limit to the power that the supercapacitor

can delivered to the MGU, as will be pointed out in the description of the simulation model. On the other hand, it would not be appropriate to size each PC on the same maximum current (and maximum power) of the supercapacitor, since the high cost increment would not be counterbalanced by an efficiency improvement of the whole KERS: the power limits imposed by each MGU, in effect, would cause the PC to work with low power factors and hence, as shown in Figure 3 of paper Part 1, with low efficiencies. The cost and the weight of each power converter was estimated on the basis of its component [57] and is also reported in Table 6.

Summing the weights and the costs of all the components of each KERS configuration, the overall commercial cost and weight of the four KERS assembly is obtained and reported in Table 7; the same table also reports the overall weight increment caused to the vehicle mass by the implementation of the KERS: as can be observed, the increment ranges from 2% to 3%, which is considered a reasonable value.

Table 7 Overall cost and weight of the four KERS considered

	KERS1	KERS2	KERS3	KERS4
Peak motor power [kW]	11.0	14.0	24.0	30.0
Commercial cost [€]	1488	1615	2146	2459
Weight [kg]	26.8	27.5	36.4	38.4
Weight increment [%]	2.0%	2.1%	2.8%	2.9%

10 Performance parameters and probability indexes

This section presents the performance parameters and indexes taken into consideration for the evaluation of the energetic and economic advantages connected to the implementation of the e-KERS proposed. Starting from the original vehicle, i.e. without KERS contribution, it is obvious that the traction power is completely delivered by the thermal engine:

$$P_{trac}(t) = P_I(t) + P_{road}(t) = P_{eng}(t) \cdot \eta_T \cdot \eta_D \tag{62}$$

Given the vehicle speed profile as function of time, the total amount of energy E_0 produced by the thermal engine to perform a complete driving cycle without KERS is hence:

$$E_0 = \int_{cycle} P_{eng}(t) \cdot dt = \int_{cycle} \frac{P_{trac}(t)}{\eta_D \cdot \eta_T} \cdot dt \tag{63}$$

In this evaluation no energy recovery is performed during the braking phases (the original vehicle is considered); moreover, being related to the vehicle dynamics only, it does not involve the engine efficiency, and hence does not represent the real energy consumption of the vehicle, which will be considered further on.

When considering the application of the KERS proposed, the driving cycle simulations were performed including the KERS mass into the vehicle mass; moreover, with the aim to nullify the effect of the initial energy content E_i of the SC, each driving cycle simulation involving the use of the KERS was iteratively repeated assuming that the energy stored in the supercapacitor at the beginning of the cycle was equal to the energy content evaluated at the end of the previous cycle simulation: the iteration was stopped when the difference between these two values resulted lower than 10J (negligible with respect to the nominal energy of the SC, i.e. 190 kJ); this procedure allowed to obtain results near a real vehicle usage on distances much longer than that of the driving cycle (0.995 km and 4.87 km for the ECE-15 and Artemis Urban respectively, as reported in Table 2)

The advantage connected to the use of the KERS was evaluated considering that, as already stated by equation (12) in paper Part 1, in the system proposed (Figure 6) the power produced by the brushless motor, reduced by the gear efficiency, contribute to vehicle acceleration reducing the power traction demand to the thermal engine:

$$P_{trac}(t) = P_I(t) + P_{road}(t) = \left[P_{MGU}(t) \cdot \eta_G + P_{eng}(t) \cdot \eta_T \right] \cdot \eta_D \tag{64}$$

According to this observation, the traction energy E_S delivered by the KERS during a driving cycle is computed as:

$$E_S = \int_{P_{MGU}>0} P_{MGU}(t) \cdot \eta_G \cdot \eta_D \cdot dt \tag{65}$$

being the brushless motor power $P_{MGU}(t)$ evaluated by equations (27) and (39) of the model presented in the paper Part 1. As indicated, this integral is restricted to the acceleration phases only, when the power delivered by the brushless motor $P_{MGU}(t)$ is positive. It results that, for the vehicle equipped with the proposed KERS, the amount of energy produced by the thermal engine to perform a complete driving cycle E_K is hence reduced to:

$$E_K = \frac{1}{\eta_D \cdot \eta_T} \left[\int_{cycle} P_{trac}(t) \cdot dt - E_S \right] = \frac{1}{\eta_D \cdot \eta_T} \int_{cycle} \left[P_I(t) + P_{road}(t) \right] \cdot dt - \frac{E_S}{\eta_D \cdot \eta_T} \tag{66}$$

It is worth noting that the integral of equation (66) differs from the integral of equation (63) because of the KERS mass added to the vehicle mass.

Since the difference E_O-E_K represents the reduction of the energy demand to the thermal engine, the **net energy saving** ε_K was evaluated as:

$$\varepsilon_K = \frac{E_O - E_K}{E_O} = 1 - \frac{E_K}{E_O} \tag{67}$$

The energy recovery effectiveness of the system proposed was evaluated comparing the traction energy reduction E_S obtained by the KERS implementation, with the maximum energy E_{MR} that could be ideally recovered during a whole driving cycle, evaluated as:

$$E_{MR} = \int_{cycle} P_{br}(t)\, dt \tag{68}$$

being the braking power $P_{br}(t)$ evaluated by equation (11) reported in paper Part 1. As obvious, this integral takes into account the braking phases only, i.e. the only phases during which a KERS can recover the vehicle kinetic energy.

The **recovering efficiency** η_K of the KERS was hence evaluated as:

$$\eta_K = \frac{E_S}{E_{MR}} \tag{69}$$

With the aim to further characterize the proposed KERS, the authors also evaluated two indexes frequently employed in the analysis of energy systems reliability, i.e. the *Loss of Load Probability* (LOLP) and the *Loss of Energy Probability* (LOEP).

A loss of load (or power) may occur during both an acceleration and a braking phase. In the first case, a loss of load occurs if the required inertial power is higher than the maximum power that the brushless motor can deliver. Assuming $p_L(t)$ to be the Boolean variable which determines if a loss of load is verified or not (i.e. $p_L(t)=1$ or $p_L(t)=0$ respectively), during an acceleration phase (i.e. $a(t)>0$):

$$p_L(t) = 1 \quad \text{if} \quad \frac{P_I(t)}{\eta_G \cdot \eta_D} > P_{MGU,\max}(t) \tag{70}$$

being the maximum MGU output power $P_{MGU,max}(t)$ evaluated trough equation (24) of the model (paper Part 1). If the inequality in equation (70) is not true, the loss of load is not verified and $p_L(t)=0$.

In a braking phase (i.e. $P_{br}(t)>0$), instead, a loss of load occurs if the braking power involves a too high input power for the generator (or for the supercapacitor); in a braking phase hence

$$p_L(t) = 1 \quad \text{if} \quad P_{br}(t) \cdot \eta_G > P_{MGU,\text{in},\max}(t) \tag{71}$$

where the maximum input power to the MGU $P_{MGU,in,max}(t)$ is evaluated by equation (46) of the model (paper Part 1). As before, if the inequality in equation (71) is not verified, no loss of load occurs and $p_L(t)=0$.

Since the LOLP index expresses the probability that the MGU or the supercapacitor will not allow a sufficient power exchange, it can be easily evaluated on the basis of the Boolean variable $p_L(t)$:

$$LOLP = \frac{\int_{cycle} p_L(t)\, dt}{\int_{cycle} dt} = \frac{\int_{cycle} p_L(t)\, dt}{\Delta t_{cycle}} \tag{72}$$

where Δt_{cycle} denotes the whole cycle duration.

The *Loss of Energy Probability* (LOEP) index is similar to the LOLP, with the difference that it is focused on the energy exchanged between the storage system and the MGU. The interest is now on the capability of the storage system to serve the MGU both in the acceleration and in the braking phases. In the KERS considered in this work, a loss of energy will occur during an acceleration phase (i.e. $a(t)>0$) if the supercapacitor reaches the minimum energy content $E_{SC,min}$ (see equation (38) of the model in paper Part 1), thus becoming unable to further supply the MGU (as therefore represented by equation (39) of the model); for the same KERS, a loss of energy will also occur if, during a braking phase ($P_{br}(t)>0$), the supercapacitor reaches its maximum storable energy $E_{SC,max}$ (see equation (55) of the model), thus becoming unable to store any extra energy that the MGU could provide (as stated by equation (56) of the model).

Assuming hence the Boolean variable $p_E(t)$ to determines if a loss of energy is verified or not (i.e. $p_E(t)=1$ or $p_E(t)=0$ respectively), for the KERS considered is:

$$p_E(t)=1 \quad \text{if} \quad \begin{cases} E_{SC}(t)=E_{SC,\min} \quad \text{AND} \quad a(t)>0 \\ \\ E_{SC}(t)=E_{SC,\max} \quad \text{AND} \quad P_{br}(t)>0 \end{cases} \tag{73}$$

If the conditions expressed in equation (73) are not true, the loss of energy is not verified and $p_E(t)=0$.

With the same meaning of the symbols, the LOEP index can be hence evaluated as:

$$LOEP=\frac{\int\limits_{cycle} p_E(t)\,dt}{\int\limits_{cycle} dt}=\frac{\int\limits_{cycle} p_E(t)\,dt}{\Delta t_{cycle}} \tag{74}$$

The closer to zero the value of these indexes are, the lower is the probability that the KERS elements cannot exchange the necessary power or energy. In principle, the best value of both performance indexes is zero, but this would imply the adoption of too expensive and heavy storage system or MGU. Due to the two limiting factors weight and cost, the element of the KERS will not allow to store all the energy (or to transfer all the power) required by the vehicle during a braking phase, and will not allow to transfer all the energy (or deliver all the power) required for the acceleration phases; not all transients will be satisfied by the components selected, and the performance indexes will give an idea of the suitability of the design performed: a low value of the indexes of probability will ensure that the energy (or the power) is adequately managed in most cases, without weighing down the vehicle and with reasonable costs.

11 Simulation results and discussions

As mentioned before, the model described was employed in numerical simulations performed using MATLAB Simulink to evaluate the energetic and economic benefit attainable by the implementation of the e-KERS proposed on the vehicle of Table 1 subjected to the speed profile of each of the two driving cycles adopted.

An example of the simulation output is given in the following figures, obtained considering the implementation of the KERS2 (i.e. with peak motor power of 14 kW). The upper graph of Figure 11 reproduces the vehicle speed and acceleration during a time interval of 40 s of the Artemis Urban cycle, while the lower graph reports the energy content of the supercapacitor together with the progress of the two Boolean variables p_L and p_E related to the probability indexes LOLP and LOEP respectively (KERS2 is considered).

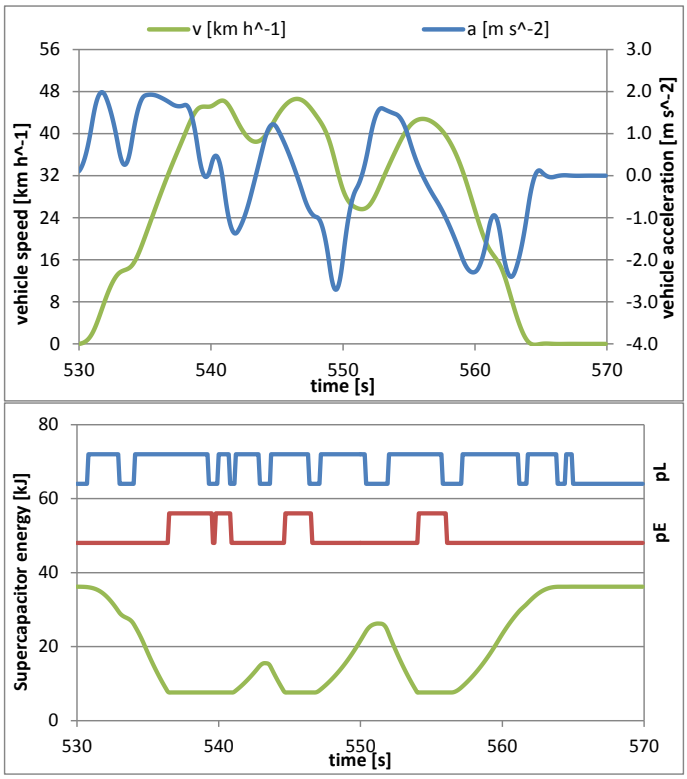

Figure 11 Upper graph: Vehicle speed and acceleration as function of time; Lower graph: Energy stored in the SC (left axis), Boolean variables p_L and p_E (right axis) as function of time. (Artemis Urban cycle, KERS2)

With reference to the same time interval, the upper graph in Figure 12 shows the progress of the inertial power required by vehicle acceleration, together with the actual and the maximum MGU output power (KERS2): it can be noted that, due to the limitations described by equations (19) to (24), the MGU is unable to follow the inertial power required by vehicle acceleration; a deeper analysis revealed the main responsible to be the low power availability from the supercapacitor: a low energy content in the SC implies a low working voltage (equation (35) of the model) which in turn causes a low power availability (equation (37)). The same Figure 12 also shows that, when the energy content of

the SC reaches the minimum level $E_{SC,min}$ (see the lower graph of Figure 11), the MGU output power becomes null, as prescribed by equation (39) of the model.

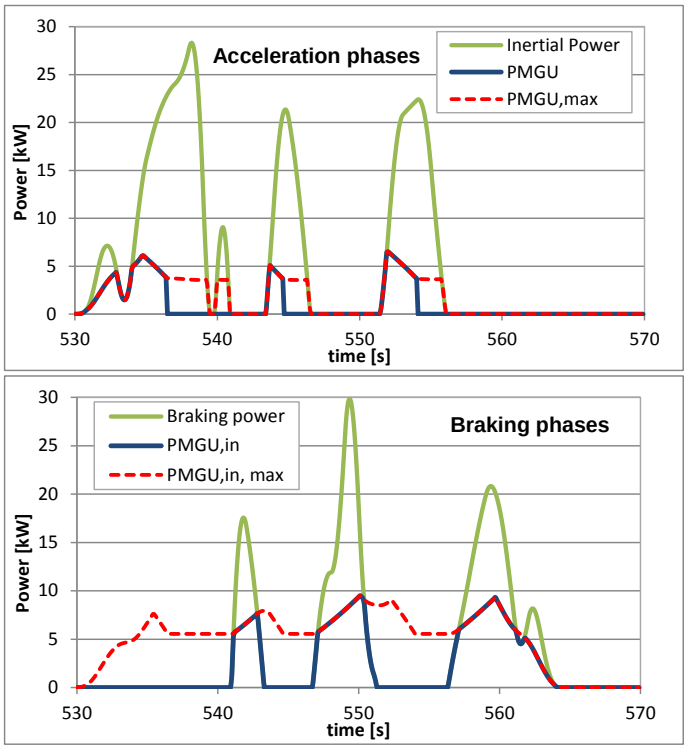

Figure 12 Upper graph: inertial power, actual and maximum MGU output power as function of time; Lower graph: braking power, actual and maximum MGU input power. (Artemis Urban cycle, KERS2)

The lower graph in Figure 12 instead reports the braking power required by the vehicle, together with the actual and the maximum input power to the brushless generator during the braking phases of the same time interval. As can be observed, the already mentioned limitations cut the power that the MGU can recover, making the maximum allowed input power significantly lower than the required inertial power. The Boolean variables reported in the lower graph of Figure 11 show that a loss of load (p_L=1) is recognized whenever the brushless machine is unable to satisfy the necessary inertial power (acceleration phases) or the required braking power (braking phases); as regards the loss of energy (i.e. p_E=1), it can be noted that, in the time interval considered, this condition occurred only when the stored energy reached the minimum level.

The graph in Figure 13 reports instead the current flowing on the DC side of the MGU controller during the Artemis Urban cycle performed with KERS2; it can be observed that, despite the high spikes, the RMS value remains well below the allowed continuous current exposed in Table 5: this confirms the suitability of the selected brushless machines, which, as already pointed out, can support peak power level from 2.4 to 3 times higher the continuous power level.

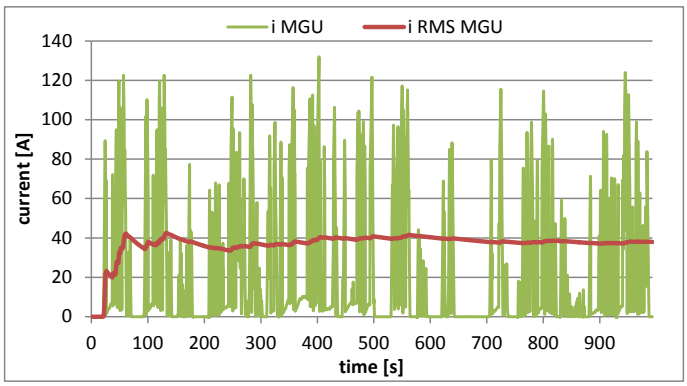

Figure 13 Brushless machine absolute instantaneous and RMS current (Artemis Urban cycle, KERS2)

The overall results of the simulations performed on the the ECE-15 driving cycle considering the four different KERS combination are reported in Table 8: as can be observed, the e-KERS proposed revealed very effective, with recovery efficiency between 47% and 40%, and energy saving between 16% and 13%. The increase of the MGU power size did not produce an advantage, since both energetic parameters significantly decreased moving from smaller to larger machines: the mild transient phases of the ECE-15 cycle could not exploit the higher power size, which instead caused both the supercapacitor and power converter to work with low power factors and hence with low efficiencies.

The probability indexes revealed low values, confirming hence the suitability of component selected for the KERS assembly; increasing the power size reduced the probability that the KERS could not satisfy the power requirement of the vehicle transient phases, thus causing a sharp decrease of the LOLP index, and at the same time accelerated the emptying of the energy storage, thus causing a slight increasing of the LOEP index.

Table 9 reports the results of the simulations performed on the Artemis Urban driving cycle. As can be observed, on a more realistic vehicle speed profile, the e-KERS produced lower recovery efficiencies (from 28% to 33%) and higher probability indexes, while the energy savings instead remained between 13% and 16%: unlike the previous case, however, increasing the power size produced a beneficial effect on both energetic parameters, which resulted maximized with KERS3. As in the previous case, the LOLP index showed a sharp reduction (from 39% to 13%) with power size increase, while LOEP index revealed a more evident increase (from 16% to 21%).

According to LOEP index results, the storage system can be considered adequately sized for urban application, being its capacity sufficient to exchange the most part of the required energy during the whole driving cycles. As regards the LOLP index, the simulations revealed that, with an proper sizing, the e-KERS is able to satisfy most of the power demand related to vehicle acceleration or braking. In conclusion, the system proved to have a good potential, since considerable recovery efficiencies and energy savings were obtained despite the components selected for the KERS assembly are not optimized for this application. Aiming to exploit the e-KERS on a real urban application, the results

obtained with the Artemis Urban cycle should be considered: according to these simulations, the best configuration for the vehicle considered (see Table 1) resulted to be KERS3, equipped with a 24 kW peak power brushless motor.

Table 8 Results obtained by simulations performed on ECE-15 driving cycle

	KERS1	KERS2	KERS3	KERS4
Peak motor power [kW]	11.0	14.0	24.0	30.0
Energy required without KERS [kJ]	398	398	398	398
Energy required with KERS [kJ]	333	334	340	346
Recovered energy [MJ]	72.6	71.6	67.5	62.5
Max recoverable energy [MJ]	152	152	153	154
Energy recovery efficiency	47.7%	47.0%	44.0%	40.7%
Energy saving	16.4%	16.1%	14.5%	13.1%
LOEP	8.28%	9.10%	9.91%	10.3%
LOLP	19.2%	12.9%	5.57%	1.54%

Table 9 Results obtained by simulations performed on Artemis Urban driving cycle

	KERS1	KERS2	KERS3	KERS4
Peak motor power [kW]	11.0	14.0	24.0	30.0
Energy required without KERS [kJ]	3006	3006	3006	3006
Energy required with KERS [kJ]	2604	2567	2525	2556
Recovered energy [MJ]	459.7	498.8	559.7	533.4
Max recoverable energy [MJ]	1673	1674	1686	1688
Energy recovery efficiency	27.5%	29.8%	33.2%	31.6%
Energy saving	13.4%	14.6%	16.0%	15.0%
LOEP	16.2%	17.3%	19.7%	21.2%
LOLP	36.7%	32.4%	17.2%	11.1%

For the evaluation of the real fuel economy connected to the use of the KERS proposed, the authors supposed that the ratio between the net and the real energy required to perform the cycle remains unchanged when evaluated with or without the contribution of the KERS: in other words, the authors supposed that the average efficiency of the internal combustion engine evaluated on the whole driving cycle remains unchanged when introducing the KERS. According to this assumption, the energy savings produced by the KERS with respect to the net energy E_0 can be extended to the real energy consumed on each driving cycle; this means, as example, that the 16% energy saving obtained in the Artemis Urban cycle with KERS3, can be also expected with respect to the real energy consumption of the vehicle. Moreover, being the real energy consumed by the vehicle derived from the fuel combustion, the same energy savings can be applied to the real fuel consumption (reported in

Table 2), thus obtaining the fuel savings reported in Table 10 and Table 11 for the two driving cycles ECE-15 and Artemis Urban respectively. It is also worth to point out that, being the CO_2 emissions related to the fuel consumed, the same percentage of fuel saving can be considered valid for the reduction of CO_2 emitted.

The assumption made obviously constitutes a simplified approach, which should be verified; two considerations, however, can be made in support of this assumption:

1) Due to air/fuel mixture formation phenomena, the spark ignition engine efficiency during an acceleration transients may result lower with respect to the steady state operation at the end of the acceleration;

2) As assumed by the authors, the KERS proposed contributes to vehicle acceleration, thus reducing the participation of the internal combustion engine to this lower efficiency phase, moving hence the most of the thermal engine application to the steady state operations, characterized by higher efficiency.

This means that the assumption made by the authors may also reveal conservative, since the ratio between the net and real energy (i.e. the average engine efficiency) could be increased by the use of the KERS, and the consequent fuel saving could hence result higher than what has been estimated.

Considering the mean European gasoline price of 1.476 € L^{-1}, obtained by the European Environment Agency [58], the estimated fuel savings were converted in the corresponding money savings, as shown in Table 10 and Table 11.

Table 10 Estimated fuel economy obtained by the e-KERS (ECE-15 driving cycle)

	KERS1	**KERS2**	**KERS3**	**KERS4**
Fuel consumption with KERS [L (100 km)$^{-1}$]	6.94	6.96	7.10	7.22
Fuel saving with KERS [L (100 km)$^{-1}$]	1.36	1.34	1.20	1.08
Money saving with KERS [€ (100 km)$^{-1}$]	2.01	1.97	1.77	1.60
KERS payback distance [km]	73965	81807	120954	153552
KERS payback time [year]	7.40	8.18	12.10	15.36
CO_2 emissions avoided [ton (10^5 km)$^{-1}$]	16.1	16.2	16.5	16.8

With the aim to make a comparison with the investment required by the KERS implementation, the estimated money savings were employed to evaluate the probable KERS payback distance, that is the distance that the vehicle has to cover before amortizing the KERS cost (reported in Table 7 for each KERS combination). The results of this evaluation is also reported in Table 10 and Table 11: as can be observed, the lower payback distances resulted to be about 73,000 km, which, for an average distance travelled of 10,000 km year^{-1}, may correspond to a payback period of about 7.3 years. The sense of this evaluation is that the implementation of the KERS proposed could produce such an economic

benefit that, after a distance travelled of about 73,000 km, the entire system cost would be balanced. From an economic point of view, the best configurations for a real urban application revealed to be KERS2 and KERS1. To further point out the potential of the KERS studied, the authors also evaluated the CO_2 emission reduction obtainable: as can be observed in the last row of both Table 10 and Table 11, for the vehicle considered, the CO_2 emissions that could be avoided (after 100,000 km) by the implementation of the KERS proposed moves between 16 and 20 tons.

Table 11 Estimated fuel economy obtained by the e-KERS (Artemis Urban driving cycle)

	KERS1	KERS2	KERS3	KERS4
Fuel consumption with KERS [L (100 km)$^{-1}$]	8.92	8.79	8.65	8.76
Fuel saving with KERS [L (100 km)$^{-1}$]	1.38	1.51	1.65	1.54
Money saving with KERS [€ (100 km)$^{-1}$]	2.03	2.22	2.43	2.28
KERS payback distance [km]	73183	72682	88212	107941
KERS payback time [year]	7.32	7.27	8.82	10.8
CO_2 emissions avoided [ton (10^5 km)$^{-1}$]	20.7	20.4	20.1	20.3

12 Sensitivity analysis

The waveforms reported in Figure 12 allow to point out that in the system proposed, both the supercapacitor and the MGU can cause inadequate power deliver (as described by equations (27) and (47) of the model): as a matter of fact, the power availability of the SC, which reduces when the energy stored decreases, or the power capability of the MGU, which instead is limited by its stall torque or by the maximum allowed peak current, may substantially limit or reduce the effectiveness of the KERS. With the aim to examine the effect of each single element of the KERS on the overall performances, a proper sensitivity analysis was carried out. The purpose of this analysis was to ascertain how limitations and inefficiencies of each KERS component affect the performance parameters (recovery efficiency and energy saving) and the performance indexes (LOEP and LOLP).

The limitations taken into account are:

1) the power limits imposed by the MGU, reported in equations (23), (24) and (27) for the acceleration phase, and in equations (45), (46) and (47) for the braking phase

2) the power limits imposed by the SC, as reported in equations (37) and (35), valid for both acceleration and braking phase.

3) the limited amount of energy storable, which may prevent the SC to supply the MGU, as described in equations (38) and (39), or to recover energy, as described in equations (55) and (56).

The inefficiencies considered regards all the three elements of the KERS, i.e.:

1) the SC, whose efficiency has been described by equation (33)
2) the MGU, whose main losses have been described in the model adopted through equation (18) for the acceleration case, and through equation (41) for the braking phase
3) the power converter, whose efficiency has been expressed by equations (30) and (31) as function of output and input power respectively.

The analysis carried out by the authors followed the classical *one-at-a-time* procedure, starting from the most ideal version of the KERS and gradually introducing the limitation or the inefficiency of each element one at a time (KERS2 was considered in this analysis). Eight different version of the KERS were hence considered, named with capital letters from A to H, reported in Table 12 together with the simulation results obtained on the Artemis Urban driving cycle:

- **Version A**: totally ideal KERS, without any power limit, without energy storage limit, and with all efficiencies=1
- **Version B**: as version A but with limited power and energy storage of the supercapacitor
- **Version C**: as version A but with limited power of the brushless machine
- **Version D**: all power and storage limitations taken into account, all efficiencies=1
- **Version E**: as version D, considering the real power converter efficiency
- **Version F**: as version D, considering the real MGU efficiency
- **Version G**: as version D, considering the real SC efficiency
- **Version H**: real KERS, with all power and storage limitations, and with all real efficiencies (KERS2)

As mentioned before, each simulation was iteratively repeated until convergence of the initial and final energy in the storage system. The first interesting result is revealed by the totally ideal KERS (version A), which, despite the recovery efficiency of 93% (as expected, the efficiency of both final drive and MGU gear forbid to reach 100%), exhibits an energy saving of 50%, which should be hence considered the reference limit, the asymptote to aim for, and obviously depends on both the driving cycle and the vehicle considered: in other words, for the vehicle adopted, in the Artemis Urban cycle the maximum recoverable braking energy amounts to 50% of the net energy required to perform the whole cycle.

Taking into account the SC limitations (in terms of both storage capacity and power limit, KERS version B) led to roughly a 26% reduction on both recovery efficiency and energy saving; considering, instead, only the MGU power limit (KERS version C), led to a 23% reduction of recovery efficiency and energy saving with respect to version A: this means that, in the system proposed, the limitations introduced by the supercapacitor resulted to have an effect even

higher than the power limits of the MGU. When simultaneously considering the limitations of both the MGU and the SC (i.e. KERS version D), the overall reduction was found to be 33% with respect to version A. As regards the performance indexes, it can be observed that, when only power limitations were taken into consideration (KERS version from A to D), LOEP index, which is related to energy, remained almost constant (10% to 8%), while the LOLP index increased by about 20% for each single limitation, and reached 29% with both limitations simultaneously (KERS version D).

Table 12 Sensitivity analysis results (Artemis Urban cycle)

	A	B	C	D	E	F	G	H
MGU Power	**100x**	**100x**	**Real**	**Real**	**Real**	**Real**	**Real**	**Real**
SC Storable Energy	**100x**	**Real**	**100x**	**Real**	**Real**	**Real**	**Real**	**Real**
SC Power	**100x**	**Real**	**100x**	**Real**	**Real**	**Real**	**Real**	**Real**
PC efficiency	**1**	**1**	**1**	**1**	**Real**	**1**	**1**	**Real**
MGU efficiency	**1**	**1**	**1**	**1**	**1**	**Real**	**1**	**Real**
SC efficiency	**1**	**1**	**1**	**1**	**1**	**1**	**Real**	**Real**
Recovery efficiency η_K	93.0%	68.5%	72.1%	62.8%	54.6%	46.9%	48.4%	29.8%
Energy saving ε_K	49.8%	36.2%	38.2%	33.0%	28.4%	24.1%	25.0%	14.6%
LOEP	9.74%	9.58%	8.46%	8.29%	10.17%	12.1%	12.2%	17.3%
LOLP	0.0%	19.3%	20.8%	28.8%	29.5%	30.5%	30.0%	32.4%

The effect of the real efficiencies of the power converter, of the brushless machine, and of the supercapacitor were taken into account one-at-a-time in the KERS version E, F and G respectively, which revealed, with respect to version D, an energy saving reduction (and hence an almost equal recovering efficiency reduction) of 14%, 26% and 23%: as can be deduced, hence, the efficiency of the power converter caused the lowest performance decrement, while the losses in the MGU and in the SC produced a stronger effect. When considering simultaneously the losses of all the KERS components (version H), the reduction of KERS effectiveness resulted 56% with respect to version D, and 71% with respect to version A. The energy losses of the KERS components caused moderate increment of the LOEP index, while the LOLP index remained almost unchanged.

The performed sensitivity analysis allowed to point out the aspect of the KERS elements which should be improved to increase the braking energy recovery. As regards the MGU, its limited power output proved to be a major cause of KERS effectiveness reduction: an optimized design should hence maximize both stall torque and peak power, being the continuous power operation less important. As regards the supercapacitor, the low working voltage associated with the

lower energy content revealed a major cause of KERS effectiveness reduction, together with its ohmic losses: better results would be obtained reducing the Equivalent Series Resistance (ESR), and above all increasing the maximum working voltages $V_{SC,max}$, which would also reduce the working currents and hence ohmic losses. As example, if a supercapacitor with a double $V_{SC,max}$ (i.e 96 V) is considered, even maintaining the same storage capacity of 190.1 kJ (the capacitance should hence be one fourth) and supposing a double ESR, the KERS2 would reach an energy saving of 17.5% and a recovery efficiency of 34.8%.

13 Conclusions

In this two-papers work the authors propose and evaluate the performance attainable by an electric KERS for internal combustion engine vehicle. The system, as detailed described in paper Part 1, was conceived to recover the vehicle kinetic energy during braking phases, to be re-used in successive vehicle acceleration phases, so as to reduce the power demand to the internal combustion engine, and, as a consequence, the related fuel consumption and pollutant emissions. The overall design of the KERS, and hence the selection of its main element, was carried out considering solutions with the minimum increase of the vehicle mass, focusing on market available products, which also allowed to evaluate the related costs. The evaluation of the benefit introduced by the implementation of the KERS proposed was carried out by means of numerical simulation performed with Matlab Simulink, considering the application of a widely diffused passenger car (1.4 L spark ignition engine, 90 kW maximum output power, 1315 kg reference mass) on two reference urban driving cycles: the ECE-15 and the more realistic Artemis Urban cycle. The sizing of the KERS components, performed through simple energetic evaluation, showed a convergence of the two reference cycles on the energy storage capacity, which, for the vehicle considered, was established to be at least 120 kJ. When focusing on the power size of the KERS, instead, the two cycles produced substantial differences, as therefore could be expected, given their different acceleration levels; as a result, 13 kW were found to be sufficient for the ECE-15, while when considering the Artemis Urban, the required power size resulted 35 kW: this result led the authors to consider four different KERS assembly (named KERS1, KERS2, KERS3 and KERS4) obtained by combining a single supercapacitor with four brushless motors of different power levels (11,14,24 and 30 kW respectively), with the aim to identify the optimal choice by means of the numerical simulation. To the purpose, a mathematical model (detailed described in paper Part 1) was realized, taking into account, for each component, the real efficiency and the energy and power constraints introduced in the system. The goodness of the design was assessed by the use of the Loss Of Load Probability (LOLP) and of the Loss Of Energy Probability (LOEP) indexes, while the energetic performances of the KERS were evaluated in terms of energy recovery efficiency (evaluated with respect to the ideally recoverable energy) and energy saving (with respect to the net energy required by the vehicle without KERS to complete a whole driving cycle). According to

the results of the simulations performed, the sizing of the energy storage revealed appropriate, as proved by the low values of LOEP obtained (about 8-10% in the ECE-15 driving cycle, and 16-21% in the Artemis Urban), which means that the elements of the KERS successfully exchanged almost all the necessary energy. As regards the power size, KERS1 and KERS2 revealed unsuitable according to the values obtained for the LOLP index (37-32% in the Artemis Urban), while KERS3 and KERS4 proved to adequately fulfil the required power transfer between MGU and supercapacitor. As concern the energetic performance, the KERS considered in the simulations revealed recovery efficiency in the order of 41-48% in the ECE-15 and 28-33% in the Artemis Urban, and energy savings of 13-16% in both driving cycles: from a purely energetic point of view, the best choice revealed to be KERS3, which maximized both energy saving and recovery efficiency in the Artemis Urban cycle. The simulations also revealed that, for the configurations considered, the weak point

Considering that to the energy saving corresponds a fuel consumption reduction, the authors also evaluated the fuel saving and the related economic advantages (given the average gasoline price in Europe) obtainable by the implementation of the KERS proposed. From an economic point of view, the best configurations for a real urban application revealed to be KERS2 and KERS1: it was estimated that economic benefits gained by their implementation on the selected vehicle could allow to balance their cost within a travelled distance of 73,000 km. To further point out the potential of the KERS studied, the authors also evaluated the CO_2 emission reduction obtainable: for the vehicle considered, it was estimated that, after 100,000 km, the avoided CO_2 emissions could amount to 20 tons.

The authors consider the results obtained really encouraging, confirming that the managing of the energy during transients by a supercapacitor based KERS can contribute to the hybridization process of internal combustion engine vehicles and is able to produce an advantage for the customer and for the environment as well.

A sensitivity analysis was also carried out, with the aim to examine the effect of each single element of the KERS on the overall performances: it was understood that, in the system proposed, the limitations introduced by the SC (power and storage capacity) determine efficiency penalization even higher than the MGU: a higher working voltage of the SC could allow to increase the energy saving by 20%.

14 References

[43] Pipitone E., Vitale G., "A regenerative braking system for internal combustion engine vehicles based on supercapacitors - Part 1: System analysis and modelling", submitted for pubblication to Journal of Power Sources, available at http://emilianopipitone.altervista.org/publication_list.htm

[44] Jisheng Hu, Yukun Zhao and Xiaojing Liu, "The design of regeneration braking system in light rail vehicle using energy-storage Ultra-capacitor," 2008 IEEE Vehicle Power and Propulsion Conference, Harbin, 2008, pp. 1-5, doi: 10.1109/VPPC.2008.4677708

[45] Ouyang, M., Zhang, W., Wang, E., Yang, F., Li, J., Li, Z., Yu, P., Ye, X., Performance analysis of a novel coaxial power-split hybrid powertrain using a CNG engine and supercapacitors, (2015) Applied Energy, 157, pp. 595-606, DOI: 10.1016/j.apenergy.2014.12.086

[46] B. Lequesne, "Automotive Electrification: The Nonhybrid Story," in IEEE Transactions on Transportation Electrification, vol. 1, no. 1, pp. 40-53, June 2015, doi: 10.1109/TTE.2015.2426573

[47] Mock P., 2018, "European vehicle market statistics 2018/2019", International Council on Clean Transportation Europe (ICCT), www.theicct.org

[48] Vock C., Hubel J., Tsokolis D., Samaras C., Ntziachristos L., Tola R., Ricci C., and Samaras Z., (2014) Report on the Development and Use of the Vehicle Energy/Emission Simulator, Deliverable D.3.2.1, ICT-EMISSIONS Consortium

[49] Barlow T.J., Latham, S., McCrae, I.S. and Boulter, P.G., (2009) A Reference Book of Driving Cycles for Use in the Measurement of Road Vehicle Emissions, Published project report, ISSN 0968-4093, HIS

[50] Giakoumis E. G., (2017) Driving and Engine Cycles, Springer International Publishing, ISBN: 783319490342 978-3-319-49034-2

[51] André M., (2004) The ARTEMIS European driving cycles for measuring car pollutant emissions, Science of the Total Environment, 334-335, pp. 73-84, DOI: 10.1016/j.scitotenv.2004.04.070

[52] UNECE, (2013) Development of a World-wide Worldwide harmonized Light duty driving Test Cycle (WLTC), UN/ECE/WP.29/GRPE/WLTP-IG, Technical Report GRPE-68-03

[53] http://www.greentechee.com/48V-165F-super-capacitor-modules-with-large-power_p41.html

[54] http://www.evdrives.com/

[55] http://motenergy.com/brdcmo2.html

[56] Dixon, J.W., Leal, I.A., (2002), “Current control strategy for brushless dc motors based on a common DC signal”, IEEE Transactions on Power Electronics, 17 (2), pp. 232-240, DOI: 10.1109/63.988834

[57] Vitale G., Pipitone E., (2019), “A Six Legs Buck-boost Interleaved Converter for KERS Application”, submitted for publication to World Electric Vehicle Journal, currently available for consultation at http://emilianopipitone.altervista.org/publication_list.htm

[58] European Environment Agency [online] https://www.eea.europa.eu/data-and-maps/indicators/fuel-prices-and-taxes/ (Accessed February 2019).

15 Symbols and abbreviations

a, $a(t)$	vehicle acceleration, as function of time t
A_f	frontal area of the vehicle
C	Capacitance
CNG	Compressed natural gas
CVT	Continuous variable transmission
c_r	rolling resistance coefficient
c_x	drag coefficient of the vehicle
E_{br}	energy that can be recovered during a braking phases
E_0	net energy demand to the thermal engine to perform a complete driving cycle without KERS
E_K	net energy demand to the thermal engine to perform a complete driving cycle with KERS
E_{MR}	maximum recoverable energy in a whole driving cycle
E_S	traction energy delivered by the MGU during a driving cycle
E_{SC}	energy stored in the supercapacitor
$E_{SC,max}$	maximum storable energy in the supercapacitor
$E_{SC,min}$	minimum allowed energy content of the supercapacitor
ECE-15	European urban driving cycle
ESR	Equivalent series resistance of the supercapacitor
EUDC	European extra urban driving cycle
F_{aer}	vehicle aerodynamic resistance
F_{br}	braking force acting on the vehicle
F_{dist}	external disturbance force acting on the vehicle
F_{grav}	force of gravity acting on the vehicle in the case of a slope
F_{road}	Road load (vehicle resistance to the movement)
F_{roll}	vehicle rolling resistance
F_{trac}	traction force acting on the vehicle
I	MGU rotor inertia
i_{MGU}	Current on the DC side of the MGU controller
$i_{MGU,\ max}$	Maximum allowed current on the DC side of the MGU controller

$i_{MGU,\,SL}$	MGU current limit imposed by the maximum power output of the supercapacitor
$i_{PC,max}$	Maximum allowed current in the power converter
i_{SC}	Current in the supercapacitor
ICE	Internal combustion engine
ICEV	Internal combustion engine vehicle
k	windage losses constant of the MGU
KERS	Kinetic Energy Recovery System
L_F	mechanical friction losses of the MGU
L_{MGU}	MGU power losses
L_R	resistive and power interrupter losses of the MGU
L_W	windage losses of the MGU
m_v	vehicle mass
MGU	Motor Generator Unit
$n_{MGU,\,max}$	Maximum rotation speed of the MGU
NEDC	New European Driving Cycle
p	tires pressure
P_{br}	braking power
p_E	Loss of energy Boolean variable
P_{eng}	power output from the internal combustion engine
P_I	Inertial power
p_L	Loss of power Boolean variable
P_{MGU}	power output from the MGU
$P_{MGU,max}$	maximum power output from the MGU
$P_{MGU,in}$	power input to the MGU
$P_{MGU,in,max}$	maximum power input to the MGU
P_{PC}	power output from the power converter
$P_{PC,max}$	maximum power output from the power converter
$P_{PC,in}$	power input to the power converter
$P_{PC,in,max}$	maximum power input to the power converter
P_{road}	road load power
P_{SC}	power output from the supercapacitor

$P_{SC,in}$	power input to the supercapacitor
$P_{SC,max}$	maximum power output from the supercapacitor
P_{trac}	traction power acting on the vehicle
PC	power converter
PMSM	permanent magnet synchronous motor
R	the resistive losses constant of the MGU
RMS	Root mean square value
R_W	vehicle wheel radius
SC	Supercapacitor
UDC	Urban driving cycle
t	time
T_F	constant friction torque of the MGU
T_{MGU}	torque delivered by the MGU
$T_{MGU, CL}$	MGU torque limit imposed by the maximum allowed current $i_{MGU,max}$
$T_{MGU, SL}$	MGU torque limit imposed by the maximum power output of the supercapacitor
$T_{MGU, stall}$	peak stall torque of the MGU
v, v(t)	vehicle speed, as function of time t
V_{MGU}	voltage on the DC side of the MGU controller
$V_{MGU, max}$	maximum allowed voltage on the DC side of the MGU controller
V_{SC}	instantaneous working voltage of the supercapacitor
$V_{SC, max}$	maximum allowed voltage of the supercapacitor
WLTC	worldwide harmonized light vehicles test cycles
x_{PC}	normalized output power from the power converter
$x_{PC,in}$	normalized input power to the power converter